LIMNOLOGY and OCEANOGRAPHY

ASLO

Limnol. Oceanogr. 9999, 2022, 1–16

doi: 10.1002/lno.12174

Pelagic and ice-associated microalgae under elevated light and pCO_2: Contrasting physiological strategies in two Arctic diatoms

Klara K. E. Wolf [1,2*] **Sebastian D. Rokitta** [1] **Clara J. M. Hoppe** [1] **Björn Rost** [1,3]

[1]Marine Biogeoscience, Alfred Wegener Institute for Polar and Marine Science, Bremerhaven, Germany
[2]Institute for Hydrobiology and Fisheries, Hamburg University, Hamburg, Germany
[3]Faculty of Biology/Chemistry, University of Bremen, Bremen, Germany

Abstract

Sea ice retreat, changing stratification, and ocean acidification are fundamentally changing the light availability and physico-chemical conditions for primary producers in the Arctic Ocean. However, detailed studies on ecophysiological strategies and performance of key species in the pelagic and ice-associated habitat remain scarce. Therefore, we investigated the acclimated responses of the diatoms *Thalassiosira hyalina* and *Melosira arctica* toward elevated irradiance and CO_2 partial pressures (pCO_2). Next to growth, elemental composition, and biomass production, we assessed detailed photophysiological responses through fluorometry and gas-flux measurements, including respiration and carbon acquisition. In the pelagic *T. hyalina*, growth rates remained high in all treatments and biomass production increased strongly with light. Even under low irradiances cells maintained a high-light acclimated state, allowing them to opportunistically utilize high irradiances by means of a highly plastic photosynthetic machinery and carbon uptake. The ice-associated *M. arctica* proved to be less plastic and more specialized on low-light. Its acclimation to high irradiances was characterized by minimizing photon harvest and photosynthetic efficiency, which led to lowered growth. Comparably low growth rates and strong silification advocate a strategy of persistence rather than of fast proliferation, which is also in line with the observed formation of resting stages under low-light conditions. In both species, responses to elevated pCO_2 were comparably minor. Although both diatom species persisted under the applied conditions, their competitive abilities and strategies differ strongly. With the anticipated extension of Arctic pelagic habitats, flexible high-light specialists like *T. hyalina* seem to face a brighter future.

In the Arctic, rapid increases in air and sea surface temperature (Timmermans et al. 2015; Maturilli et al. 2019) accelerate the thinning and retreat of sea ice (Wadhams 2012; IPCC 2021). In currently still ice-covered regions, a transition trend from multi- to first-year-ice can be observed, with overall earlier ice breakup, melting of the light-reflective snow cover, as well as formation of melt ponds. These phenomena profoundly increase the irradiance intensity and variability, which is one of the most important drivers of productivity, not only in the upper ocean water column but also in under-ice habitats (Hill et al. 2018; Lannuzel et al. 2020; Nicolaus et al. 2012). Furthermore, rising atmospheric CO_2 partial pressure (pCO_2) causes ocean acidification, which is especially pronounced in the Arctic because of low temperatures and lower buffering capacities of the freshening sea water (AMAP 2018; Zhang et al. 2020).

Since food webs depend critically on photosynthetic primary producers, the described environmental transitions will likely affect many other organisms in the trophic network, such as invertebrates, fish larvae and ultimately also top predators (Søreide et al. 2010). Diatoms are the dominant primary producers in the Arctic (Armbrust 2009) and occupy diverse niches, including the open ocean as well as sea-ice. In line with these niches, recent studies found diatoms to follow different strategies to cope with changing environmental drivers, like light and pCO_2 (Croteau et al. 2021; Joli et al. 2021; Kvernvik et al. 2021).

A prime challenge for photosynthetic cells is to maximize photon (i.e., energy) harvest, while simultaneously minimizing damage to the photosynthetic apparatus caused by excess light energy. To achieve this, photoacclimation processes take place

*Correspondence: klara.wolf@awi.de

Additional Supporting Information may be found in the online version of this article.

Author Contribution Statement: KW performed data acquisition, KW and SR analyzed the raw data, KW drafted the first version of the manuscript. All authors KW, SR, CH, and BR contributed substantially to the study's conception, to improving the manuscript and approved its final version.

on time scales from seconds to days (Moejes et al. 2017). For example, the potential for photon harvest can be adjusted by changing pigment composition, controlling antenna size, and connectivity, as well as by dissipation of excess energy as heat, so-called non-photochemical quenching (NPQ). In the next step, the "harvested" energy is converted to reductive energy, as electrons are stripped from water and forwarded into the photosynthetic electron transport chain. Here, an "overreduction" can occur, and potentially harmful excess electrons need to be dissipated through a number of biochemical processes. For example, electrons can be fed back to oxygen to form either water (via the so-called Mehler reaction) or reactive oxygen species for which a number of detoxification systems are available in the cell (Foyer et al. 2009).

To achieve balanced growth, not only energy capture, but also downstream cellular processes, e.g., nutrient assimilation, carbon fixation, and macromolecule synthesis need to be adjusted and tuned to maximize the efficiency of the photosynthetic light reactions (Huner et al. 1998). Biochemical mismatches or imbalances can cause cellular "stress" and are costly to deal with. They can arise, for instance, from the kinetics of RubisCO, the key enzyme for carbon fixation, which suffers from slow turnover rates, especially at cold temperatures (Young and Schmidt 2020). Psychrophilic diatoms can compensate for this by expressing higher amounts of this enzyme (Gerecht et al. 2019), but protein biosynthesis is expensive in terms of energy as well as nitrogen resources, inducing a tradeoff between resource expenditure and the maximization of C-fixation (Young et al. 2015). The ability of microalgae to cope with different kinds of photosynthetic stress has been shaped over evolutionary timescales by the selective pressures experienced in the habitats they occupy. Accordingly, ice-associated algae typically struggle to cope with the high light (HL) intensities and the variability that occurs in open ocean waters (e.g., Kvernvik et al. 2020, 2021; Croteau et al. 2021). Pelagic species, on the other hand, have developed plastic photosynthesis apparatuses and effective protective mechanisms to thrive under such light regimes (Lacour et al. 2018; Kvernvik et al. 2020; White et al. 2020).

Effects of pCO_2 in diatoms are known to be small compared to other taxa, highly species-specific (Gao and Campbell 2014), and often interact with other drivers, especially with light (Li and Campbell 2013; Hoppe et al. 2015; Seifert et al. 2020). More specifically, elevated pCO_2 often stimulates photosynthesis and growth under low light (LL), while it can decrease it under HL (Gao et al. 2019). CO_2 effects are commonly explained with reallocation of energy among competing processes, which is also why they are modulated by the availability of energy, i.e., light. Under pre-industrial and contemporary aquatic CO_2 concentrations, CO_2 is potentially limiting the rate of carbon fixation by RubisCO, and most algae, therefore, employ so-called CO_2-concentrating mechanisms (CCMs) that utilize the chemiosmotic gradient of photosynthesis to accumulate CO_2 in the vicinity of RubisCO (Rokitta et al. 2022). Since CCMs consume less chemiosmotic energy under the higher pCO_2 expected for the future, cells can profit from more energy available to photosynthesis (Rokitta et al. 2012; Van de Waal et al. 2019). At the same time, more energy may be required to maintain pH homeostasis within the cell under acidified conditions, together causing an optimum curve of CO_2 response (Bach et al. 2011).

To investigate the responses of pelagic and ice-associated microalgae to the anticipated environmental changes, we chose two ecologically important species: *Thalassiosira hyalina*, a pelagic diatom that frequently dominates Arctic spring blooms, including ice-edge blooms (von Quillfeldt 2000; Hegseth and Sundfjord 2008), and has demonstrated high physiological plasticity toward changes in temperature, pCO_2, and light (Kvernvik et al. 2018; Wolf et al. 2018, 2019). *Melosira arctica* is known for forming long strands under multi-year sea-ice (Gran 1904; Syvertsen 1991; Melnikov et al. 2002) and can contribute disproportionally to carbon export to the deep ocean (Boetius et al. 2013), especially during ice-melt and breakup. To the best of our knowledge, no detailed ecophysiological investigations on *M. arctica* have been published to date, which is surprising considering its large contribution to under-ice biomass and carbon export, and thus its relevance for modeling efforts of ice-algal biomass production (e.g., Castellani et al. 2017; van Leeuwe et al. 2018).

In this study, physiological strategies of these two species were investigated through their acclimated responses to a matrix of two different light (LL = 50 and HL = 300 μmol photons m^{-2} s^{-1}) and pCO_2 regimes (380 and 1000 μatm pCO_2). The LL level resembles an average irradiance in a wind-mixed pelagic habitat, or at the bottom of first-year ice and snow cover in late spring; the HL level was chosen to resemble a situation in a more stratified surface open ocean, or that during ice break-up and melt pond formation in summer (Nicolaus et al. 2012; Hill et al. 2018). The pCO_2 treatments resemble current and end-of-the-century pCO_2 conditions under a high-emission scenario. Based on their ecological niches, we expected *T. hyalina* to profit from HL and to experience only minor CO_2 effects, as observed in preceding studies (Wolf et al. 2018). *M. arctica* was expected to photosynthesize more efficiently under LL and to flexibly respond to changing carbonate chemistry, which tends to vary more strongly within dense aggregates under the ice compared to pelagic realm (McMinn et al. 2014). In addition to conventional analyses of growth, elemental composition and Chlorophyll *a* (Chl *a*) quota, we applied fast-repetition rate fluorometry (FRRF) and performed gas-flux measurements via membrane-inlet mass spectrometry (MIMS) to unravel photophysiological adjustments on a qualitative and quantitative level. The physiological strategies investigated here elucidate physiological mechanisms through which these species are adjusting to their environment, and thus allow a glimpse at how well each of them

may cope with the conditions to be expected in a future Arctic ocean.

Materials and methods

Culture conditions and experimental setup

T. hyalina and *M. arctica* cultures were obtained as single-cell isolates from the Kongsfjord, Svalbard (78°55′N, 11°56′E; isolated in 2014, strain WFB1) and from the central Arctic ocean (79° 33.23′N, 4° 50.29′W; isolated in 2015, strain PS93.1_030), respectively. Experiments were conducted in 2015/2016 as semi-continuous batch cultures in sterile 1-L glass bottles. In order to minimize changes in carbonate chemistry, to ensure nutrient-replete conditions throughout the experiments, and to remain close to natural population densities, cultures were diluted every 2–6 d, depending on cell density (*T. hyalina* max. 10,000 cells mL^{-1}, *M. arctica* max. 4000 cells mL^{-1}, i.e., up to 45 μg Chl *a* L^{-1}). Sampling and dilution was conducted under sterile conditions, using a laminar flow hood. Cells were cultivated in 0.2-μm sterile-filtered Arctic seawater (salinity 33.5) enriched with macronutrients (100 μmol L^{-1} NO_3^-, 6.2 μmol L^{-1} HPO_4^{2-}, 100 μmol L^{-1} $SiOH_4$), vitamins, and trace metals according to f/2 media (Guillard & Ryther, 1962). Experiments were performed in a temperature-controlled (3°C) room, with bottles immersed in water-filled aquaria for additional temperature stability. Continuous surveillance with a temperature logger (Almemo 2890, Ahlborn) ensured temperature stability at 3.4 ± 0.15°C.

Cells were grown under continuous light using daylight lamps (Biolux T8, 6500K, Osram). Irradiance levels were adjusted with a black mesh fabric and measured using a 4π sensor and data logger (ULM-500, Walz). Species were grown in a matrix of low and high light (LL vs. HL, 50 ± 1 vs. 300 ± 4 μmol photons m^{-2} s^{-1}) and low and high pCO_2 (380 vs. 1000 μatm). The four resulting treatments (HL380, HL1000, LL380, LL1000) were tested with $n = 4$ biological replicates of each strain (except for *T. hyalina* LL where $n = 3$). In a side experiment with a reduced set of measured parameters, *M. arctica* was also cultured under the same conditions but at intermediate light (110 μmol photons m^{-2} s^{-1}). Prior to the experimental phase, all cultures were acclimated to treatment conditions for at least 6 d until growth rates stabilized (> 7 generations).

Carbonate chemistry

Cultures were continuously aerated (~170 mL min^{-1}) with humidified air of target pCO_2 delivered through sterile 0.2-μm air-filters (Midisart 2000, Sartorius Stedim), provided by a custom-built gas mixing system (*see* Hoppe et al. 2015). Additionally, the growth medium was equilibrated (≥ 24 h) to the target pCO_2 at the respective temperature prior to inoculation. Stability of carbonate chemistry throughout the experiment was monitored by regular measurements of pH using a three-point calibrated electrode and logger system (Aquatrode plus Pt1000/pH 826 logger, Metrohm). The full cabonate system (Supplementay Table S1) was calculated for 3°C on the basis of pH and DIC values using the program CO2sys (Pierrot et al. 2006) with dissociation constants of carbonic acid by Mehrbach et al. (1973), refitted by Dickson and Millero (1987), as well as dissociation constants for sulfuric acid obtained by Dickson (1990). Samples of dissolved inorganic carbon (DIC) were taken on the day of final sampling, gently filtered through 0.2-μm cellulose-acetate syringe-filters (Sartorius Stedim), and stored head-space free in 5-mL gas-tight borosilicate bottles in darkness at 3°C. DIC was measured colorimetrically in duplicates, according to the method of Stoll et al. (2001) with a QuaAAtro autoanalyzer (Seal Analytical), and corrected using Certified Reference Materials (A. Dickson, Scripps Institution of Oceanography). Cell-free control bottles with sterile medium were incubated alongside culture bottles, and provided baseline values of pH and DIC. Deviations in DIC from the incubations compared to these abiotic control bottles were typically ≤2%.

Growth, cellular composition, and production

Growth rates of *T. hyalina* were determined by monitoring cell densities using a Coulter Multisizer III cell counter (Beckman-Coulter). Since *M. arctica* cell-chains tend to entangle, this species' growth rates were based on measurements of Chl *a* concentration in cultures over time (details see ahead). In both cases, specific growth rates μ (d^{-1}) were calculated by the formula $\mu = (lnN_t - lnN_0)/\Delta t$, where N_t refers to cell density or Chl *a* concentration at time t, N_0 to the initial cell density or Chl *a* concentration, and Δt to the passed time (in days) since the start of the incubation. For each culture, we used the mean value of exponential fits of all cell densities or Chl *a* concentrations of two or more consecutive dilution cycles (each spanning 3–6 d, example see Supporting Information Fig. S2).

Cell counts of *M. arctica* were performed for filtration time-points on an inverse light microscope (Axio Observer, Zeiss) in 10-mL Uthermöhl-chambers. We hereby also distinguished between regular cells and cells of divergent morphology. The latter exhibited < 50% of regular size, had a more oval cell shape, and were often brighter in color (Supporting Information Fig. S1a), resembling descriptions of resting stages in Kaczmarska and Jahn (2006). Since scanning electron micrographs of the silica frustules supported this interpretation (Supporting Information Fig. S1b), they are in the following referred to as resting stages.

For growth rate estimation and at the end of each incubation, Chl *a* samples were filtered on glass fiber filters (GF/F, 0.7-μm nominal pore size; Whatman), shock-frozen in liquid nitrogen, and stored at −80°C. For analysis, filters were shredded in acetone (90%) with glass beads (0.5–1 mm diameter) in a homogenizer (Precellys Evolution, Bertin Technologies). After overnight extraction at 4°C, Chl *a* was measured fluorometrically (TD-700, Turner Designs), including an acidification

step (1 M HCl) (Knap et al. 1996). For particulate organic carbon (POC) and nitrogen (PON), cells were filtered onto precombusted (15 h, 500°C) GF/F filters, stored at −20°C, and then dried at 60°C. POC analysis was performed using a gas chromatograph CHNS-O elemental analyzer (Euro EA 3000, HEKAtech).

POC production rates per cell were obtained by multiplication of the respective elemental quota with corresponding growth rates μ [pg POC cell^{-1} d^{-1}]. In addition, Chl *a*-specific POC production was calculated for better comparison with O_2 and inorganic carbon fluxes by normalizing cellular POC production with the Chl *a* quota of the respective replicate, yielding [mg C (mg Chl *a*)$^{-1}$ h^{-1}].

Variable Chl *a* fluorescence

Chl *a* variable fluorescence and derived photosynthesis vs. irradiance (PI) curves of relative PSII electron transfer rates were measured using a Fast Ocean FRR fluorometer (FRRF, FastOcean PTX) combined with a FastAct system (Chelsea Technologies). Prior to the assays, samples of *T. hyalina* and *M. arctica* were dark-acclimated inside the FastAct chamber for at least 10 min. The excitation wavelength of the fluorometer was set to 450 nm. The FRRF was used in single turnover mode, with a saturation phase comprising 100 flashlets of 2-μs pitch and a relaxation phase comprising 40 flashlets of a 50-μs pitch. The minimum (F0) and maximum chlorophyll fluorescence (Fm) was derived from iterative fitting of the induction phase (Kolber et al. 1998) and the relaxation phase (Oxborough et al. 2012). The maximum dark-acclimated quantum yield was calculated after Krause and Weis (1991) as Fv/Fm = (Fm − F0)/Fm. Relative electron transfer rates through PSII in the light were calculated accordingly as rETR = (F′m − F′0)/F′m *PAR. The nonregulated Y(NO) and regulated Y(NPQ) non-photochemical quenching was determined after Klughammer and Schreiber (2008) at 400 μmol photons m^{-2} s^{-1} (except for *M. arctica* at LL, where it was measured at 570 μmol photons m^{-2} s^{-1}), which were saturating light levels for cultures in all treatments. Additional parameters like the reopening rate (τ), absorption cross section (i.e., antenna size, σ), and connectivity between reaction centers (ρ) were estimated in the dark-acclimated state following Kolber et al. (1998) and Oxborough et al. (2012).

Gas-exchange measurements

To assess the microalgae's cellular exchange of O_2 and inorganic carbon (C_i) in PI curves, MIMS was applied following the approach of Badger et al. (1994) with modifications described in Kottmeier et al. (2016*a*). This approach is based on continuous measurements of O_2 and CO_2 during consecutive light–dark intervals, and makes use of the chemical disequilibrium during light-dependent C_i uptake to differentiate between CO_2 and HCO_3^- fluxes across the plasmalemma. The custom-built MIMS consists of a light-adjustable and temperature-controlled 8-mL cuvette, which is coupled to a sector-field multicollector mass spectrometer (Isoprime, GV Instruments) via a gas-permeable 0.01-mm polytetrafluorethylene-membrane (Reichelt Chemietechnik). After passing through the membrane, O_2 and CO_2 are conducted into the mass spectrometer so that the photosynthetic and respiratory fluxes of these gases can be monitored during light and dark phases, respectively.

Algal cells were concentrated by gentle filtration using polycarbonate filters (3-μm pore-size; Merck Millipore) and washed two times with 10 mL DIC-free F/2 R medium (buffered to the respective culturing pH using 50 mM HEPES) to exchange the media. Afterward, the concentrated cell culture was transferred to the pre-cooled cuvette. $NaHCO_3^-$ solution was added to final concentrations of 2.1 mmol L^{-1} to establish normal DIC backgrounds, while dextran-bound sulfonamide was added to final concentrations of ~ 25 μmol L^{-1} to suppress potential activities of extracellular carbonic anhydrase, which ensures that a chemical disequilibrium can develop during illumination. After a pre-acclimation step (3–6 min of LL followed by 6 min of darkness), PI-curves were assessed in 6-min light : dark cycles with increasing light intensities. During the transfer into the assay buffer and cuvette, cells were kept at the incubation temperature ± 1°C.

Net photosynthesis was determined from the steady-state O_2 fluxes at the end of the light phase, while respiratory O_2 uptake was measured during the subsequent dark phase. Photosynthetic and respiratory O_2 fluxes were converted to C_i fluxes by applying a photosynthetic quotient of 1.3 (Spilling et al. 2015) and a respiratory quotient of 1.0, respectively (Burkhardt et al. 2001; Rost et al. 2007). Cellular CO_2 uptake rates were derived from the rate of CO_2 depletion during steady-state photosynthesis at saturating light levels, which were further corrected for the simultaneous interconversion between CO_2 and HCO_3^- under the respective chemical disequilibrium. Cellular HCO_3^- uptake was calculated from a mass balance equation, i.e., the difference between net photosynthetic C_i uptake and net CO_2 uptake. All rates were normalized to Chl *a* concentration in the cuvette. For further details on the calculations of the photosynthetic fluxes, please refer to Badger et al. (1994) and Kottmeier et al. (2016*a*).

Estimation of photosynthetic parameters (PI-curves)

Both FRRF and MIMS assess photosynthesis, but while FRRF describes the relative electron transport from photosystem II, approximating gross photosynthesis, the MIMS measures O_2 fluxes, including the mitochondrial respiratory activity, hence net photosynthesis. To accommodate for the different measures of those methods and still use the same fit function for both, we modified a function from Platt et al. (1980) to allow for respiration (i.e., "negative" photosynthesis rates at light intensities below the compensation point) as well as an inhibition term to depict photophysiological stress at high irradiances:

$$V = \left(V_{\max;\text{theor}} \times \left(1 - e^{\left(\frac{-\alpha \times I}{V_{\max;\text{theor}}} \right)} \right) \times e^{\left(\frac{-\beta \times I}{V_{\max;\text{theor}}} \right)} \right) + \text{Resp} \quad (1)$$

$$V_{\max} = V_{\max;\text{theor}} \times \left(\frac{\alpha}{\alpha+\beta} \right) \times \left(\frac{\beta}{\alpha+\beta} \right)^{\left(\frac{\beta}{\alpha} \right)} \quad (2)$$

$$I_k = \frac{V_{\max}}{\alpha} \quad (3)$$

$$I_{Inh} = \frac{V_{\max;\text{theor}}}{\alpha} \times ln\left(\frac{\alpha+\beta}{\beta} \right) \quad (4)$$

In this photosynthesis function, I is the incident irradiance, while $V_{\max;\text{theor}}$ represents a theoretical value of maximum photosynthesis, which would be approached in absence of light inhibition. $V_{\max}$ represents the apparent maximum photosynthesis rate, I_k the irradiance where the curve transitions from light limitation to light saturation, and α is the initial light-limited slope, also known as the maximum light-use efficiency. The parameter β represents the inhibition coefficient, I_{Inh} the irradiance where photoinhibition begins, and Resp represents the respiration, i.e., "negative" O_2 evolution in darkness ($I = 0$). After obtaining the parameters of the PI-curves, the equation can be solved for $V = 0$ in order to obtain the compensation point c, i.e., the irradiance where photosynthesis exactly balances respiration. Values for the photosynthesis at acclimation irradiance (V_{accli}) were obtained by using the curve parameters and entering the irradiance values during acclimation in the LL and HL treatments, respectively. In order to differentiate between the photosynthetic parameters based on electron transport (FRRF) and O_2 evolution (MIMS), the respective parameters are distinguished by a subscript (i.e., α_e, $V_{max;e}$, $I_{k;e}$ and α_{O2}, $V_{max;O2}$, $I_{k;O2}$).

Data handling and statistics

All parameters were statistically tested using two-way-ANOVA (R Core Team, 2017, version 4.0.2) to identify the effects of light and CO_2 treatments, as well as their interaction (significance level ≤ 0.05). Data were tested for normality (Levene's test > 0.05) and homogeneity (Shapiro–Wilk test > 0.05), using log transformation of data where assumptions were violated. Only few parameters, derived from FRRF measurements in *M. arctica*, were not normally distributed ($I_{k;e}$, $V_{max;e}$, α_e, Fv/Fm, ρ). An overview of all statistical results is provided in Supplementary Table S3. Correlations between ratios of resting stages and growth or stoichiometric parameters of *M. arctica* were based on data in the LL and HL treatment, as well as the side experiment at an intermediate light level, and tested using simple linear models in the R-software. One biological replicate (B) of *M. arctica* in the HL-380 treatment was strongly dominated by resting stages (72%), while the other replicates had very low resting stage abundance (3%–9%). We removed this outlier from further analysis of cell properties to prevent a large distortion in this treatment.

Results and discussion

T. hyalina: opportunistic all-rounder with high plasticity

Physiological stability under both light regimes

In *T. hyalina*, specific growth rates (μ) remained stable between 0.8 and 0.9 d^{-1} under all tested conditions (Fig. 1a), suggesting that fast growth has a high priority, which may be an advantageous competitive strategy of this species. Cellular POC quotas, however, were significantly higher under HL conditions (+ 65%, $p = 0.002$, Supplementary Table S2), and thus cellular POC production increased (+ 60%, $p < 0.001$, Fig. 1b). Slightly increased C : N ratios (from 5.1 to 5.2, $p = 0.04$, Supplementary Table S2) and stable BSi : POC ratios of 0.3 ($p = 0.12$; Fig. 1f) suggest that both, N-acquisition and silification, were upregulated alongside with C-fixation under HL to maintain biomass stoichiometry. This hints toward a controlled investment of additional energy into the buildup of cellular biomass under high irradiance, which has previously been observed in *T. hyalina* (Kvernvik et al. 2020) as well as in other pelagic diatom species (Thompson et al. 1991).

Chl *a* : POC ratios were reduced under HL ($p < 0.001$, Fig. 1e), which is a typical response to elevated light (Kvernvik et al. 2020; Lewis et al. 2018; MacIntyre et al. 2002). As the Chl *a* quota remained unaltered ($p = 0.11$, Fig. 1d), however, this photoacclimation was driven by changes in POC quotas. Increased light thus fueled higher biomass production per cell in *T. hyalina*, while most other cellular parameters remained stable despite a six-fold increase in irradiance. Not only Chl *a* quotas but also other fluorescence-derived parameters of rETR at PSII (i.e., Fv/Fm, $V_{max;e}$, $I_{k;e}$, τ, σ, ρ; see Fig. 2 and Supplementary Table S2) remained remarkably unaltered in our treatments. Hence, acclimation did not occur on the level of light harvesting, nor did we observe signs of substantial light stress, as values of maximum quantum yield (Fv/Fm, Fig. 2a) remained unaffected. Similarly, non-photochemical quenching (Y(NPQ), Fig. 2b) remained unchanged, without upregulation of photoprotective energy dissipation in the antennae (i.e., the xanthophyll cycle).

Overall, our data for *T. hyalina* implies that larger energy input under HL are directly invested into C-fixation and biomass buildup without prominent signs of stress, which is in line with the previous finding for this species by Kvernvik et al. (2020). The stability in properties other than C-fixation, however, also means that photosynthetic efficiency was not further increased under LL. Such a "non-responsive" light-harvesting system will generate electrons according to incident light and thus yields opportunistically high energy input when the environment allows, without investing resources into costly photophysiological adjustments.

HL acclimation as a ground state, modulated by respiration

Along with Chl *a* quota, also antenna size (approximated as σ, Fig. 2c) remained stable across treatments, suggesting also constant light-harvesting efficiency of reaction centers and

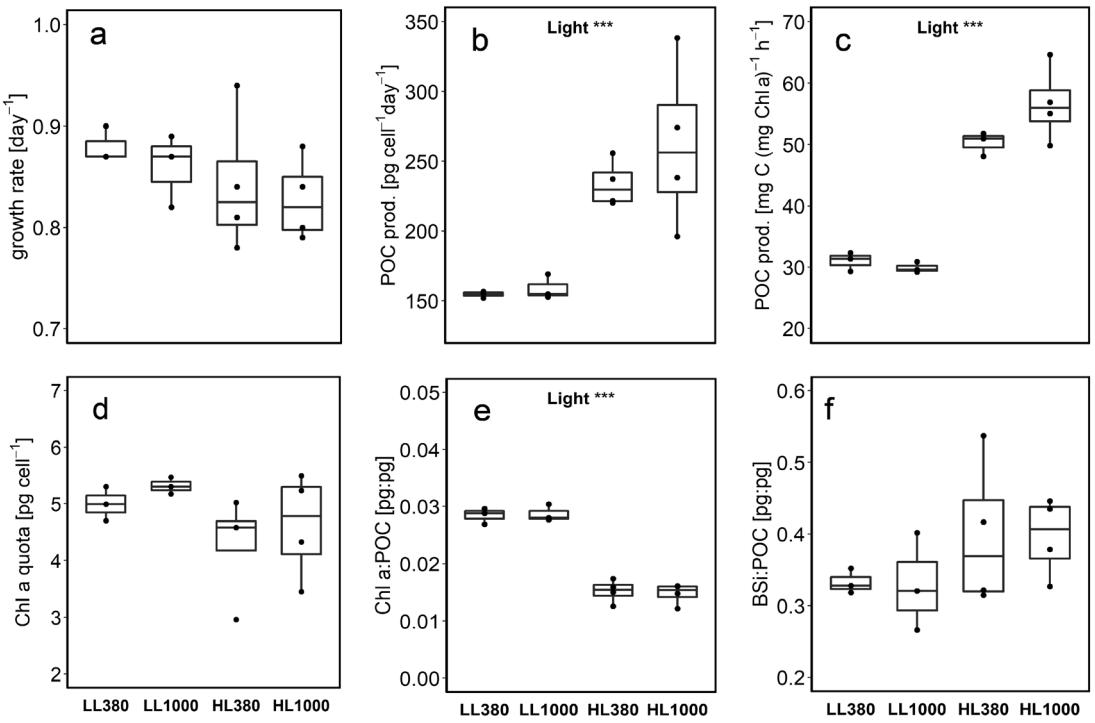

Fig. 1. Stoichiometric and growth responses of *T. hyalina* in the four treatments (LL/HL = low/high light, 380/1000 = μatm pCO_2). Points around boxplots show biological replicates. Significant differences between light or CO_2 treatments are marked in the title as follows: *** < 0.001; ** < 0.01; * < 0.05. Abbreviations: BSi: biogenic silica; Chl *a*: chlorophyll *a*; POC: particulate organic carbon.

thus making trends in Chl *a*-specific MIMS data comparable to RCII-specific FRRF data (despite not knowing specific RCII to Chl *a* ratios). As expected, net photosynthesis under acclimation irradiance, as measured by MIMS, was significantly higher under HL ($V_{accli;O2}$ + 80%; Fig. 1m, $p < 0.001$), and was remarkably well aligned with the observed increase in Chl *a*-specific POC production (+ 86%, Fig. 2g, Supplementary Table S2). This roughly doubled net photosynthesis under HL, however, does not match the almost tripled electron transport rate ($V_{accli;e}$, Fig. 2d). Furthermore, while the maximal light-use efficiency of photochemical energy (α_e, Fig. 2e) remained stable across light treatments, the maximum light-use efficiency of net photosynthesis (α_{O2}) was significantly lower in HL compared to LL ($p < 0.001$, Fig. 2h). While the former observation could potentially also suggest a change in the ratio of PSII per Chl *a*, both of these apparent discrepancies between electron transport and production rates could be explained by the strongly stimulated dark respiration (+ 260%, $p < 0.001$; Fig. 2k), which likely consumed larger parts of the photosynthate generated in HL-acclimated cells. Accordingly, photosynthesis seems to become less efficient under HL conditions (trends in Chl *a*-specific POC production and $V_{accli;O2}$ compared to trends in $V_{accli;e}$, Fig. 2d vs. 2g) and the initial light-limited slope of O_2 production is lowered (α_{O2}, Fig. 2h), since the relative amount of photosynthetic energy consumed by respiration is larger at the lower photosynthetic rates under low incident light. The strongly elevated dark respiration suggests that HL-acclimated cells had an increased metabolic demand, even independently of acute incident light. This may reflect higher maintenance costs of the higher biomass per cell itself (POC quota +- 65%, Supplementary Table S2), higher energy-consuming detoxification mechanisms, or enhanced photosystem turnover in the HL treatment (Apel and Hirt 2004; Campbell and Serôdio 2020).

Under saturating light, maximum net O_2 production ($V_{max;O2}$) and C_i uptake ($V_{max;Ci}$) was similar in all treatments (~ 120–150 μmol C (mg Chl *a*)$^{-1}$ h^{-1}, $p = 0.07$, Supplementary Table S2). While HL-acclimated cells nearly reached these maximum rates under acclimation conditions, LL-acclimated cells could only build up biomass at a lower C_i uptake rate. Accordingly, HL-acclimated cells exhibited light acclimation values below the acclimation irradiance ($I_{k;e}$ ~ 135 μmol photons m^{-2} s^{-1}, $I_{k;O2}$ ~ 150–180 μmol photons m^{-2} s^{-1}, Fig. 2f,i), i.e., experienced light saturation at growth conditions. I_k values of LL-acclimated cells, on the other hand, were far above acclimation irradiance ($I_{k;e}$ ~ 135 μmol photons m^{-2} s^{-1}, $I_{k;O2}$ in LL ~ 95–130 μmol photons m^{-2} s^{-1}), i.e., they had grown in the light-limited part of the PI-curve. This explains why biomass production under HL was elevated (POC production,

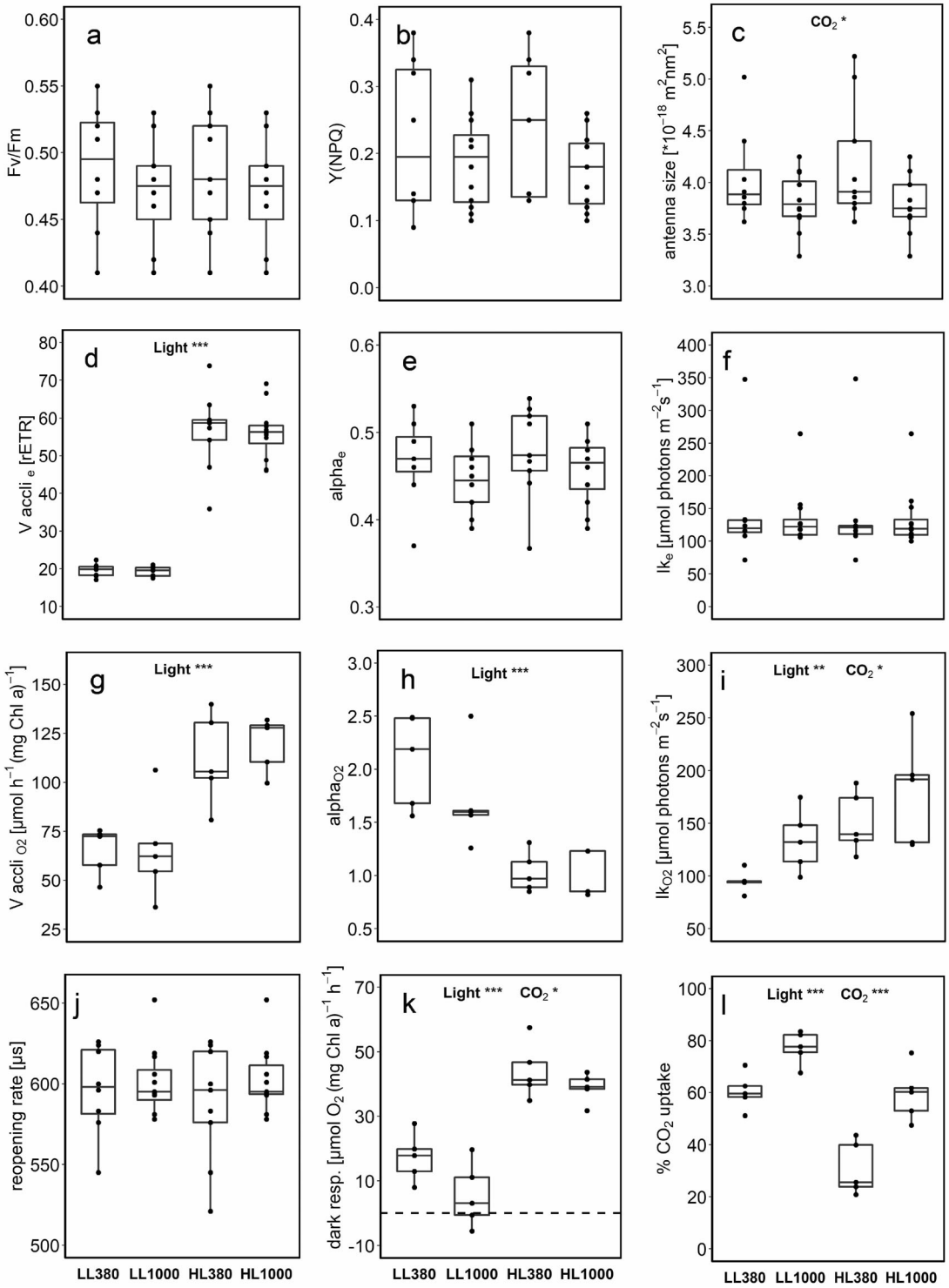

Fig. 2. Responses in rate measurements of *T. hyalina* in the four treatments (LL/HL = low/high light, 380/1000 = μatm pCO_2). Points around boxplots show replicate measurements. Significant differences between light or CO_2 treatments are marked in the title as follows: *** < 0.001; ** < 0.01; * < 0.05. Abbreviations: dark resp.: dark respiration; Vaccli: e-transport rate/ O_2 production at culturing conditions; Y(NPQ): regulated photochemical quenching. Y(NPQ) was measured at 400 μmol photons m^{-2} s^{-2}, the unit for $alpha_e$ is rETR (μmol photons m^{-2} s^{-1})$^{-1}$, for $alpha_{O2}$ μmol O_2 h^{-1} mg Chl a^{-1} (μmol photons m^{-2} s^{-1})$^{-1}$.

Fig. 1b), and underlines once more that even LL-acclimated cells are ready to use sudden increases in incident light for C-fixation.

All this advocates that HL conditions are rather the "comfort zone" of *T. hyalina*, and that this species' light-harvesting systems are maintained ready for high irradiances at all times.

They thus avoid the danger of high-light stress, while accepting light limitation under LL conditions, under which cells coped well by lowering respiration as well as their carbon quota.

Flexible carbon acquisition helps minimizing CO_2 effects

Maximum net photosynthesis ($V_{max;O2}$) and total C_i uptake ($V_{max;Ci}$) remained similar in both pCO_2 treatments (Supplementary Table S2), but *T. hyalina* flexibly adjusted their relative uptake rates of CO_2 vs. HCO_3^-. Under HL, where cells were acclimated to a higher carbon demand, HCO_3^- uptake was significantly upregulated (i.e., relative CO_2 uptake decreased by one third, $p < 0.001$, Fig. 2l), while under high CO_2 conditions, a significantly larger percentage of inorganic carbon was taken up as CO_2 (LL: from 60% to > 80%; HL: from 30% to > 60%; $p < 0.001$, Supplementary Table S2). CCM regulation was thus affected by both, light as well as pCO_2, which is in agreement with findings that CO_2 and HCO_3^- uptake systems are regulated as a function of carbon demand and supply (Rost et al. 2006*b*; Kottmeier et al. 2016*a*). In the coccolithophore *Emiliania huxleyi*, for instance, increased carbon demand under HL was met by stronger CCM activity based on HCO_3^- uptake, while acidified conditions inhibit HCO_3^- transport into the cell (Kottmeier et al. 2016*b*).

Regarding traits other than those related to the CCM, CO_2 effects were minor or completely absent. Respiration rates, for instance, were slightly lower under elevated pCO_2 in both light levels ($p = 0.03$. Fig. 2k), which could be attributed to a general down-regulation of mitochondrial activity under low pH (Strobel et al. 2013; Melzner et al. 2020). Furthermore, slightly higher irradiances were necessary to saturate photosynthesis at high CO_2 ($I_{k;O2}$, $p = 0.037$, Fig. 2i): lower respiration and easier carbon acquisition under high pCO_2 may be responsible for the slightly higher maximum O_2 production ($V_{max;O2}$, Supplementary Table S2), but these energy demands were met only at irradiances higher than acclimation conditions. Otherwise, no significant interactions between light and pCO_2 treatments were observed here, which is unlike some other diatoms, where higher pCO_2 stimulated growth and primary production under LL conditions or reduced photoinactivation at HL levels (Gao et al. 2012 and references within; Li and Campbell 2013). In an experiment testing the effect of sudden exposure to HL treatments (20 vs. 380 μmol photons m^{-2} s^{-1}) under similar pCO_2 treatments, effects of elevated CO_2 were found to be much stronger (Kvernvik et al. 2020). Thus, some of those stress responses may be transient and disappear during the acclimation process, or may only become apparent under these slightly larger spreads in light levels.

Overall, *T. hyalina* showed only weak acclimation responses to LL conditions, and instead remained "photosynthetically fit" and ready for coping with and profiting from sudden increases in irradiances. Although this strategy may not be maximizing energy output under LL conditions, it had no impact on their growth rate due to the high plasticity in carbon quota. Plasticity toward changing pCO_2 levels was also large, and the flexible CCM regulation according to their own demand and environmental supply may aid this species in achieving this robust acclimation with correspondingly little changes in traits over a wide range of environmental conditions.

Melosira arctica: low-light specialist with insufficient photoprotection

Resting stage formation under LL

M. arctica showed high variability among replicates in most parameters, especially in LL-acclimated cells, which correlates with a significant fraction of resting stages (up to 30%, Supporting Information Fig. S1c). While HL cultures contained up to 6% resting stages, a side experiment under intermediate light (110 μmol photons m^{-2} s^{-1}) contained an intermediate fraction (3%–13%, Supporting Information Fig. S1c), suggesting a light dependence of resting stage formation. One of the eight HL replicate bottles contained 70% of resting stages and was treated as an outlier. Notably, growth rate and the percentage of resting stages showed a weakly positive correlation (Supporting Information Fig. S1d; $p = 0.05$), contradicting the notion that these cells are mostly inactive (McQuoid and Hobson 1996). Variability in cell quotas (Chl *a*, POC, PON) were overall higher in treatments with high number of resting stage (i.e., the LL treatments), while variability for C : N and Chl *a* : POC ratios was consistently low in all treatments (Fig. 3, Supplementary Table S2). BSi : POC ratios showed a higher degree of silification in cultures with higher number of resting stages (Supporting Information Fig. S1e, $p = 0.02$), which is in line with resting spores often having thicker cell walls than vegetative cells (McQuoid and Hobson 1996; Ellegaard and Ribeiro 2018).

High trait variability and little gain from higher light

In contrast to the pelagic *T. hyalina*, the ice-associated *M. arctica* significantly decreased its growth rate under HL conditions from 0.6 to 0.4 d^{-1} ($p < 0.001$, Fig. 3a), implying a reduced competitiveness in terms of proliferation. Average cell quotas and POC production rates showed larger variability between the LL replicates that contained a high fraction of resting stages, and therefore no significant light effects could be determined (Fig. 2b, Supplementary Table S2). This is in contrast to *T. hyalina*, which strongly increased its POC production under HL. Biomass stoichiometry of *M. arctica* was also more variable than in *T. hyalina*, e.g., C : N ratios were significantly elevated under HL ($p < 0.001$, Supplementary Table S2). This was due to a decrease in N quota rather than an increase in C quota (Supplementary Table S2), suggesting N-assimilation and related processes may have been hampered. *M. arctica* exhibited on average five-fold higher BSi : POC ratios than *T. hyalina* (1.8 vs. 0.4; Fig. 3f). Slower growth often coincides with stronger silification in diatoms

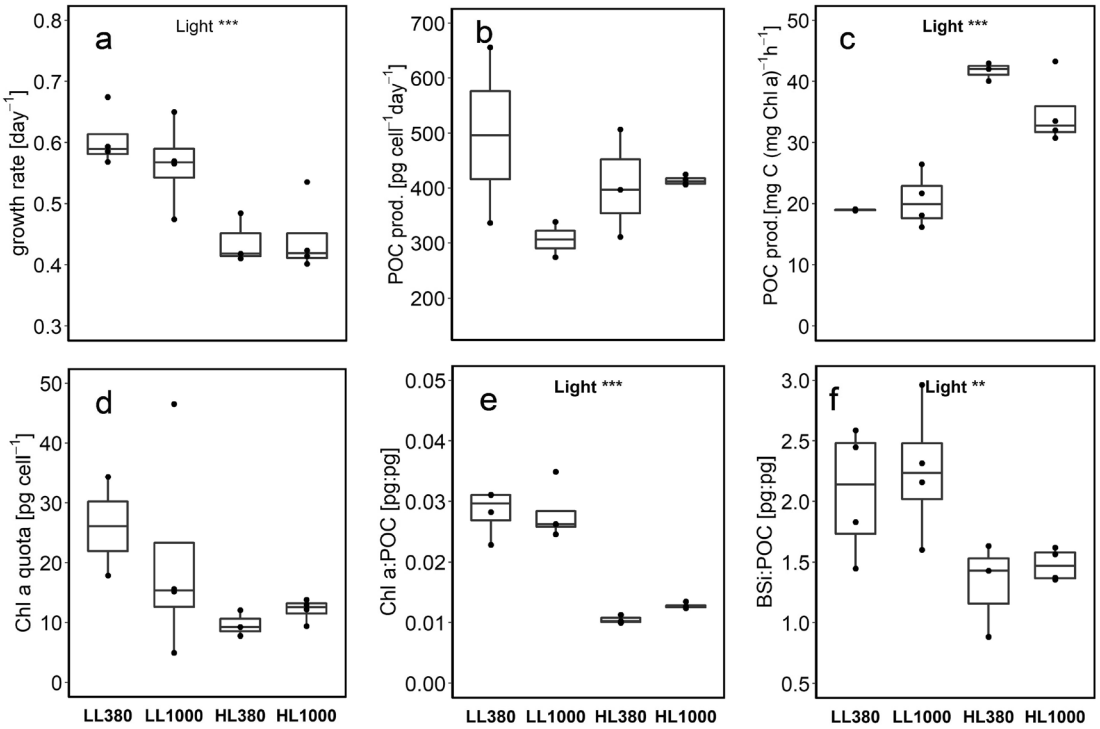

Fig. 3. Stochiometric and growth responses of *M. arctica* in the four treatments (LL/HL = low/high light, 380/1000 = μatm pCO_2). Points around boxplots show individual replicates. Significant differences between light or CO_2 treatments are marked in the title as follows: *** < 0.001; ** < 0.01; * < 0.05. Abbreviations: BSi: biogenic silica; Chl *a*: chlorophyll *a*; POC: particulate organic carbon.

(Martin-Jézéquel et al. 2000), which could indicate that grazing defense is prioritized over fast proliferation in *M. arctica*. Furthermore, BSi : POC content was increased under LL (+ 33% BSi : POC, $p = 0.007$, Supplementary Table S2), which is likely attributable to the high amount of resting stages.

Chl *a* : POC ratios were less variable than respective quotas, and were significantly reduced by ~ 60% in HL-acclimated cells ($p < 0.001$, Fig. 3e). While a similar reduction in *T.hyalina* (~ 50% Chl *a* : POC, Fig. 1e) was driven by an increase of POC quota, in *M. arctica*, this was due to reduced pigment content rather than stimulation of biomass production (Fig. 3d, Supplementary Table S2), indicating the cells' attempt to reduce energy input. Such a typical photoacclimation response (Brunet et al. 2011) is well in line with other studies on ice algae (Hegseth 1992) and indicates that HL acclimation in *M. arctica* is also more focused on preventing photodamage than exploiting elevated light availability.

Electron transport rates under acclimation light intensity (V_{acclie}) approximately doubled in response to HL (rising from 20 to 50; $p < 0.001$, Fig. 4d). Notably, also Chl *a*-specific net photosynthesis ($V_{accliO2}$) increased to a similar degree (Fig. 4g; reaching rates close to those of *T. hyalina*, Fig. 2g), and also Chl *a*-specific POC production increased accordingly (Fig. 3c). The similar effect sizes in these three parameters are remarkable, since values originate from different measurement techniques, which assess vastly different timescales (seconds to days). When normalizing these parameters to POC, however, i.e., taking the decrease in Chl *a* quota into account, these effects disappeared, showing that there was no effect of light on biomass production (POC production per cell and per POC, Supplementary Table S2). This is also in line with the variable but substantially increased dark respiration under HL (+ 72% $p = 0.07$, Fig. 4k). Hence, the HL acclimation of *M. arctica* involves throttling its photosynthetic performance via decreased Chl *a* content rather than exploiting increased energy availability.

High-light stress in spite of acclimation

In contrast to *T. hyalina*, and somewhat counterintuitively, maximum electron transport rates were significantly lower under HL than under LL ($V_{max;e}$ − 61%, $p < 0.001$, Supplementary Table S2). This was also mirrored in lower light acclimation indices under HL than under LL ($I_{k;e}$, $p < 0.001$, Fig. 4f), which suggests that HL-acclimated cells capped their light harvest far below treatment conditions, at around 100 μmol photons m^{-2} s^{-1}. LL-acclimated *M. arctica* cells thus continued to harvest incoming photons at irradiances far beyond their acclimation light, while in HL-acclimated cells, Chl *a* quota where drastically lowered in order to prevent excessive excitation pressure and oxidative stress. This is in line with the significantly downregulated absorption cross-section per RCII in the HL treatment (antenna size, $p < 0.001$, Fig. 4c).

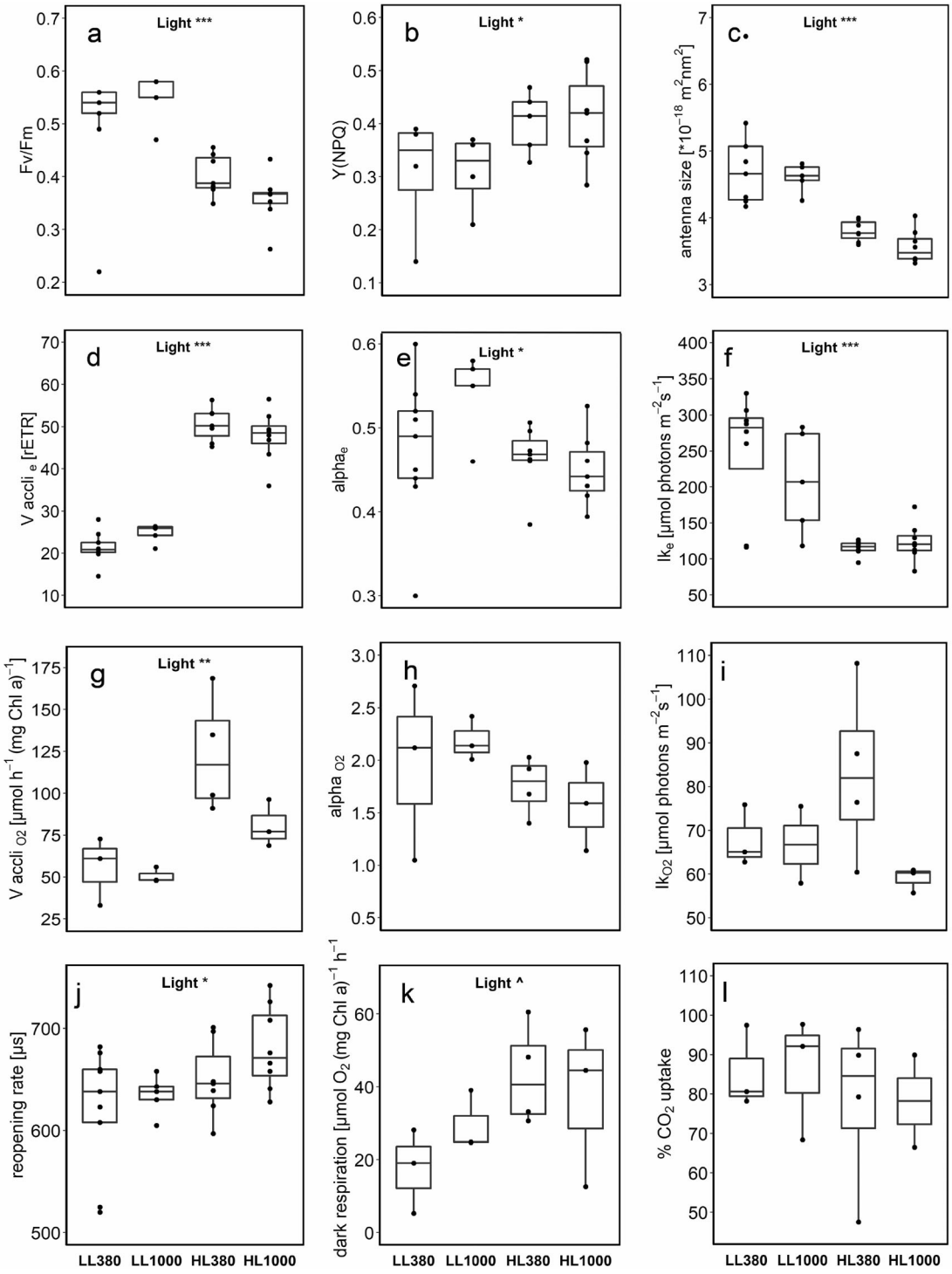

Fig. 4. Responses in rate measurements of *M. arctica* in the four treatments (LL/HL = low/high light, 380/1000 = μatm pCO_2). Points around boxplots show individual replicates. Significant differences between light or CO_2 treatments are marked in the title as follows: *** < 0.001; ** < 0.01; * < 0.05; ^ < 0.1. Abbreviations: dark resp.: dark respiration; Vaccli: e-transport rate/ O_2 production at culturing conditions; Y(NPQ): regulated photochemical quenching. Y(NPQ) was measured at 400-μmol photons m^{-2} s^{-2} (in LL treatments at 570-μmol photons m^{-2} s^{-2}), the unit for α_e is rETR (μmol photons m^{-2} s^{-1})$^{-1}$, for α_{O2} μmol O_2 h^{-1} mg Chl^{-1} (μmol photons m^{-2} s^{-1})$^{-1}$.

Accordingly, the maximum net photosynthesis ($V_{max;O2}$, Supplementary Table S2) remained unchanged by light treatment, since this parameter was normalized to Chl *a*. Taking the lower Chl *a* content into account by normalizing rates to cell or POC, also net photosynthesis followed this trend of lower maximal values in HL acclimation (data not shown). In other

words, HL-acclimated *M. arctica* set an upper limit to its maximum energy input by employing smaller antenna complexes and lower Chl *a* content, while LL-acclimated cells maintained a highly efficient harvesting machinery, aiming at maximizing photosynthetic yield at the cost of a higher risk for photodamage.

Evidence of *M. arctica* being exposed to high-light stress and possible photodamage even in the HL-acclimated state can be found in the potential photochemical efficiency of dark-acclimated cells (Fv/Fm), which was significantly decreased in HL compared to LL conditions ($p < 0.001$, Fig. 4a). One protective way to channel surplus light energy away from photochemistry, and thus to avoid potential damage, is heat dissipation, or non-photochemical quenching. This can occur in a regulated way, e.g., via the xanthophyll cycle (Y(NPQ)) or in a non-regulated way, e.g., through passive dissipation, mainly due to closed PSII reaction centers (Y(NO), Klughammer and Schreiber 2008). For *M. arctica*, regulated NPQ was only slightly higher in HL conditions compared to LL (Y(NPQ), $p = 0.02$, Fig. 4b), but approximately twice as high as in *T. hyalina* (Fig. 2b). This suggests that regulated heat dissipation played a role in its acclimation response and thus in limiting the maximal electron transport during sudden light increases, as seen in other ice algae (Croteau et al. 2021; Kvernvik et al. 2020).

Non-regulated NPQ (Y(NO), Supplementary Table S2), on the other hand, remained stable, suggesting that sudden high-light exposure did not block reaction centers, and potential photodamage may instead occur further down in the electron transport chain. Concomitantly, turnover time of PSII (reopening rate τ) was increased in HL- compared to LL-acclimated cells ($p = 0.03$, Fig. 4j). Thus, acclimation to HL did not yield a more efficient downstream machinery, as could be expected in response to increased energy input (Barlow et al. 1988), but rather became more inefficient, e.g., due to substrate limitations during C-fixation (see ahead). Insufficient capacities of the downstream processes have the potential for detrimental overreduction in the photosynthetic electron transport chain, e.g., resulting in cytotoxic ROS production (Apel and Hirt 2004). The lack of photophysiological protection against light variability under LL conditions, along with the apparent light stress in HL even after acclimation, leaves the impression of a species neither well adapted to fluctuating, nor to stable high-light regimes.

No pCO_2 effects in spite of inflexible carbon acquisition

Unlike other ice-algal species (Kvernvik et al. 2020), *M. arctica* showed no significant responses to ocean acidification, or any interactive effects of pCO_2 with light (Supplementary Table S3). This supports findings by Torstensson et al. (2021), who found assemblages of sea-ice algae dominated by *M. arctica* to be insensitive toward pCO_2 perturbations. In line with this, maximum carbon uptake rates per Chl *a* were stable in all treatments (~ 90 μmol (mg Chl *a*)$^{-1}$ h^{-1}, Supplementary Table S2) and *M. arctica* relied mainly on CO_2 uptake instead of adjusting its preferred carbon species (Fig. 4l). Such an unaltered C_i uptake behavior may also limit the ability to match higher carbon demands under increasing light (Rost et al. 2006*a*; Hoppe et al. 2015). Thus, it may be the origin of a slower photosynthetic downstream machinery, i.e., the increased reopening rate (and decreased Fv/Fm) under HL. This was in contrast to *T. hyalina*, which changed its carbon source and exhibited higher C_i uptake rates, suggesting an overall less efficient and dynamic regulation of photosynthesis in *M. arctica*. Another reason for slow downstream machinery under HL might be a rate limitation imposed by slow Rubisco kinetics at low temperatures (*see* Young et al. 2015). This is unlikely, however, as the culturing temperature was comparably high for an ice-algae like *M. arctica*.

Overall, *M. arctica* was physiologically less performant under HL than under LL, exhibiting decreased growth and signs of photophysiological stress. In contrast to *T. hyalina*, considerable acclimation to the different light levels took place, mainly through restructuring of light-harvesting antenna to maximize the energy input under LL, while minimizing it under HL conditions.

Ecological implications

T. hyalina exhibited the typical physiology of a species relying on fast proliferation, and seemed especially well equipped for high and variable irradiances. These properties are characteristic for pelagic "boom and bust" species (Assmy and Smetacek 2009) and enable them to occupy their ecological niche: similar to other ecological r-strategists often found in unstable high-nutrient environments (Prosser et al. 2007; Southwood et al. 1974), *T. hyalina* prioritizes fast growth as soon as enough light is available in early spring and while nutrients are still plentiful to develop large bloom events (von Quillfeldt 2000).

Furthermore, acclimation to LL appeared minimal, which is a good strategy when thriving in the upper mixed water column, where light regimes are rapidly fluctuating, and damage by sudden increases in irradiance is likely. Accordingly, *T. hyalina* keeps its photosynthetic apparatus extremely stable under different conditions, but plastic enough to cope efficiently with fluctuations and to profit from favorable conditions. In line with this, (Kvernvik et al. 2020) could show that *T. hyalina* uses potent protective mechanisms (e.g., xanthophyll cycle and oxidative stress defense) to overcome sudden increases in irradiance within less than 48 h without experiencing disadvantages. Furthermore, *T. hyalina*'s ability to adjust the fraction of HCO_3^- and CO_2 uptake (i.e., CCM regulation) allows for efficient C_i fixation, independently of CO_2 supply and its internal C-demands. This may also help diatoms like *T. hyalina* to thrive in dynamic mixed layers by fulfilling quickly changing carbon demands and thus preventing photodamage (Hoppe et al. 2015). Rising temperatures in

the water column may further fuel the fast growth rates of this species, as it has been shown to have a thermal optimum at temperatures above common Arctic temperatures (Wolf et al. 2018).

T. hyalina's strategy can be summarized as an opportunistic approach to the tradeoffs of growing in the sunlit mixed layer: rather than investing into fine-tuned photoacclimation to LL conditions, which entails the danger of photodamage during suddenly peaking irradiances, *T. hyalina* ensures stable growth, but otherwise endures phases of light limitation (e.g., by lowering its carbon quota) while waiting for better conditions, e.g., for a shoaling of the mixed layer.

M. arctica, on the other hand, showed rather opposite strategies and preferences. Growth rates were generally lower than those of *T. hyalina* and decreased even further in HL conditions. Acclimation to high irradiance involved mainly photoprotection rather than exploitation of the higher energy input, and nevertheless, cells showed signs of stress. In an LL-acclimated state, *M. arctica* possessed an efficient light-harvesting system, but showed little tolerance toward light fluctuations. Slow C_i uptake and growth require less investment into CCM regulation, but this adaptation may limit capacities to balance high energy inputs. *M. arctica* is typically not exposed to high or strongly fluctuating light in its sub-ice habitat, where it forms long, mucilaginous threads that grow into the underlying water column (Melnikov et al. 2002). Therefore, its physiology is tuned for optimal light harvest under stable LL conditions, often even far below the here applied irradiance (Castellani et al. 2021). High or fluctuating light situations would mainly be found in a breakup or melt-pond scenario, when the ice disintegrates and the heavy algae mats sink quickly, leading to massive, pulsed carbon export (Boetius et al. 2013).

These ecological considerations may also explain the conspicuous formation of resting stages. Traditionally, resting stage formation is thought to be initiated by nutrient-limitation, high cell densities or other kinds of non-favorable conditions (McQuoid and Hobson 1996; Pelusi et al. 2020). In the case of *M. arctica*, however, resting stage formation was found in their rather favored LL treatment, while under higher, more stressful light conditions they were nearly absent (Supporting Information Fig. S1c). As high irradiance in the sea-ice habitat is an indicator of ice-breakup, however, production of resting stages under LL conditions seems more reasonable: it allows their preservation in multi-year ice or ridges, where *M. arctica* is often found (Syvertsen 1991; Poulin et al. 2014). Another unexpected observation was that resting stages differed from vegetative cells mainly in their size (i.e., cell quota) and their BSi : POC ratio, but not in terms of other elemental ratios and even growth rates. Although SEM images showed typical morphology of resting stages (Kaczmarska and Jahn 2006; Supporting Information Fig. S1), this poses the question whether these cells were indeed *resting*, or whether the difference between a vegetative and a resting state may be rather gradual. According to our data, their main adaptation may be the stronger grazing protection, which would primarily reduce loss rates once the cells are in an environment not permitting growth (e.g., darkness). To which extend these cells actively contribute to overall growth rates remains yet to be understood.

Low growth rates, extremely strong silicification, and high percentages of resting stages under favorable conditions, all of this suggests that *M. arctica* follows a k-like strategy of slow, but optimized growth and persistence rather than one of fast, opportunistic proliferation. In comparison to pelagic species, ice-associated species have on the one hand increased encounter rates with grazers (Kohlbach et al. 2016), but on the other hand smaller loss terms due to sinking. Strong silicification can thus be used as a grazer defense without the tradeoff of fast sinking.

In conclusion, *T. hyalina* showed characteristics that explain its success as a dominant spring bloom species in northern waters. As they cope well with ocean acidification and strongly benefit from higher irradiance, this species is likely to profit from the larger areas of open, sunlit ocean as the sea ice retreats. Their final success, however, will also strongly depend on other variables such as nutrient conditions, temperature, and especially on the respective response of their direct competitors and grazers. In contrast, *M. arctica* seemed to require low irradiances and stable light conditions. Both, their photophysiology as well as their ecological strategy of forming thick, grazer-protected mats under the ice, seem disadvantageous in view of anticipated changes in the Arctic. Although *M. arctica* is traditionally described as a dweller in multi-year ice (Syvertsen 1991), there are also frequent observations in first-year and new ice, and even floating aggregates at the halocline and between ice floes (Gran 1904; Poulin et al. 2014). Nevertheless, in view of its specialized physiology, it seems likely that the relevance of this currently important Arctic biomass producer will decline alongside the retreating sea-ice, making it one of the "losers" of climate change.

Data availability statement

The data supporting the findings of this study are openly available in the Pangea Database https://www.pangaea.de/.

References

AMAP. 2018. Human health in the arctic: The Arctic Monitoring and Assessment Programme. AMAP Assessment 2018: Arctic Ocean Acidification, Tromsø, Norway.

Apel, K., and H. Hirt. 2004. Reactive oxygen species: Metabolism, oxidative stress, and signal transduction. Annu. Rev. Plant Biol. **55**: 373–399. doi:10.1146/annurev.arplant.55.031903.141701

Armbrust, E. V. 2009. The life of diatoms in the world's oceans. Nature **459**: 185–192. doi:10.1038/nature08057

Assmy, P., and V. Smetacek. 2009. Algal blooms, p. 27–41. *In* M. Schaechter [ed.], Encyclopedia of microbiology. Elsevier.

Bach, L. T., U. Riebesell, and K. G. Schulz. 2011. Distinguishing between the effects of ocean acidification and ocean carbonation in the coccolithophore *Emiliania huxleyi*. Limnol. Oceanogr. **56**: 2040–2050. doi:10.4319/lo.2011.56.6.2040

Badger, M. R., K. Palmqvist, and J.-W. Yu. 1994. Measurement of CO_2 and HCO_3^- fluxes in cyanobacteria and microalgae during steady-state photosynthesis. Physiol. Plant. **90**: 529–536. doi:10.1111/j.1399-3054.1994.tb08811.x

Barlow, R. G., and and others. 1988. Photoadaptive strategies in sea-ice microalgae. Mar. Ecol. Prog. Ser. **45**: 145–152. doi:10.3354/meps045145

Boetius, A., and and others. 2013. Export of algal biomass from the melting Arctic Sea ice. Science **339**: 1430–1432. doi:10.1126/science.1231346

Brunet, C., G. Johnsen, J. Lavaud, and S. Roy. 2011. Pigments and photoacclimation processes. *In* Phytoplankton pigments: Characterization, chemotaxonomy and applications in oceanography. Cambridge Press University.

Burkhardt, S., G. Amoroso, U. Riebesell, and D. Sultemeyer. 2001. CO_2 and HCO_3^- uptake in marine diatoms acclimated to different CO_2 concentrations. Limnol. Oceanogr. **46**: 1378–1391. doi:10.4319/lo.2001.46.6.1378

Campbell, D. A., and J. Serôdio. 2020. Photoinhibition of photosystem II in phytoplankton: Processes and patterns, p. 329–365. *In* A. W. D. Larkum, A. R. Grossman, and J. A. Raven [eds.], Photosynthesis in algae: Biochemical and physiological mechanisms. Springer International Publishing.

Castellani, G., and and others. 2021. Shine a light: Under-ice light and its ecological implications in a changing Arctic Ocean. Ambio **51**: 307–317.

Castellani, G., M. Losch, B. A. Lange, and H. Flores. 2017. Modeling Arctic sea-ice algae: Physical drivers of spatial distribution and algae phenology. J. Geophys. Res. Oceans **122**: 7466–7487. doi:10.1002/2017JC012828

Croteau, D., and and others. 2021. Contrasting non-photochemical quenching patterns under high light and darkness aligns with light niche occupancy in Arctic diatoms. Limnol. Oceanogr. **66**: S231–S245. doi:10.1002/lno.11587

Dickson, A. G. 1990. Standard potential of the reaction: AgCl (s) + ½ H2(g) = Ag(s) +HCl(aq), and the standard acidity constant of the ion HSO4- in syntheticseawater from 273.15 to 318.15 K. Journal of Chemical Thermodynamics **22**: 113–127. doi:10.1016/0021-9614(90)90074-Z

Dickson, A. G., and F. J. Millero. 1987. A comparison of the equilibrium constants for the dissociation of carbonic acid in seawater media. Deep-Sea Res. **34**: 1733–1743. doi:10.1016/0198-0149(87)90021-5

Ellegaard, M., and S. Ribeiro. 2018. The long-term persistence of phytoplankton resting stages in aquatic 'seed banks'. Biol. Rev. **93**: 166–183. doi:10.1111/brv.12338

Foyer, C. H., A. J. Bloom, G. Queval, and G. Noctor. 2009. Photorespiratory metabolism: Genes, mutants, energetics, and redox signaling. Annu. Rev. Plant Biol. **60**: 455–484. doi:10.1146/annurev.arplant.043008.091948

Gao, K., J. Beardall, D.-P. Häder, J. M. Hall-Spencer, G. Gao, and D. A. Hutchins. 2019. Effects of ocean acidification on marine photosynthetic organisms under the concurrent influences of warming, UV radiation, and deoxygenation. Front. Mar. Sci. **6**: 322. doi:10.3389/fmars.2019.00322

Gao, K., and D. A. Campbell. 2014. Photophysiological responses of marine diatoms to elevated CO_2 and decreased pH: A review. Funct. Plant Biol. **41**: 449–459. doi:10.1071/FP13247

Gao, K., E. W. Helbling, D.-P. Häder, and D. A. Hutchins. 2012. Responses of marine primaryproducers to interactions between ocean acidification, solar radiation, and warming. Mar. Ecol. Prog. Ser. **470**: 167–189. doi:10.3354/meps10043

Gerecht, A. C., G. K. Eriksen, M. Uradnikova, and H. C. Eilertsen. 2019. High ribulose-1,5-bisphosphate carboxylase/oxygenase content in northern diatom species. bioRxiv: 569285. doi:10.1101/569285

Gran, H. H. 1904. Diatomaceae from the ice-floes and plankton of the Arctic Ocean (Scientific Results of the Norwegian North Polar Expedition). Longmans, Green & Company, p. 3–74.

Guillard, R. R. L., and J. H. Ryther. 1962. Studies of marine planktonic diatoms. I. Cyclothella nana Hustedt and Detonula confervacea Cleve Canadian Journal of Microbiology **8**: 229–239. doi:10.1139/m62-029

Hegseth, E. N. 1992. Sub-ice algal assemblages of the Barents Sea: Species composition, chemical composition, and growth rates. Polar Biol. **12**: 485–496. doi:10.1007/BF00238187

Hegseth, E. N., and A. Sundfjord. 2008. Intrusion and blooming of Atlantic phytoplankton species in the high Arctic. J. Mar. Syst. **74**: 108–119. doi:10.1016/j.jmarsys.2007.11.011

Hill, V. J., B. Light, M. Steele, and R. C. Zimmerman. 2018. Light availability and phytoplankton growth beneath Arctic Sea ice: Integrating observations and modeling. J. Geophys. Res. Oceans **123**: 3651–3667. doi:10.1029/2017JC013617

Hoppe, C. J. M., L. M. Holtz, S. Trimborn, and B. Rost. 2015. Ocean acidification decreases the light-use efficiency in an Antarctic diatom under dynamic but not constant light. New Phytol. **207**: 159–171. doi:10.1111/nph.13334

Huner, N. P. A., G. Öquist, and F. Sarhan. 1998. Energy balance and acclimation to light and cold. Trends Plant Sci. **3**: 224–230. doi:10.1016/S1360-1385(98)01248-5

IPCC. 2021. Climate change 2021: The physical science basis. Contribution of Working Group 14 I to the Sixth Assessment Report of the Intergovernmental Panel on Climate Change; Technical Summary. *In* V. Masson-Delmotte [ed.], Human influence on the climate system. Intergovernmental Panel on Climate Change.

Joli, N., T. Lacour, N. J. Freyria, S.-J. Royer, M. Babin, and C. Lovejoy. 2021. Two versions of short-term phytoplankton ecophysiology and taxonomic assemblages in the Arctic Ocean's north water (Canada, Greenland). J. Plankton Res. **43**: 126–141. doi:10.1093/plankt/fbab009

Kaczmarska, I., and R. Jahn. 2006. Taxonomic appraisal of *Melosira arctica* Dickie and description of a new variety (Bacillariophyta). Bot. Mar **49**: 151. doi:10.1515/BOT.2006.020

Klughammer, C., and U. Schreiber. 2008. Complementary PS II quantum yields calculated from simple fluorescence parameters measured by PAM fluorometry and the saturation pulse method. PAM Appl. Notes **1**: 201–247.

Knap, A., A. Michaels, A. Close, D. H., and A. E. Dickson. 1996. Protocols for the Joint Global Ocean Flux Study (JGOFS) Core Measurements, JGOFS Report no. 19. UNESCO.

Kohlbach, D., M. Graeve, B. A. Lange, C. David, I. Peeken, and H. Flores. 2016. The importance of ice algae-produced carbon in the Central Arctic Ocean ecosystem: Food web relationships revealed by lipid and stable isotope analyses. Limnol. Oceanogr. **61**: 2027–2044. doi:10.1002/lno.10351

Kolber, Z. S., O. Prasil, and P. G. Falkowski. 1998. Measurements of variable chlorophyll fluorescence using fast repetition rate techniques. I. Defining methodology and experimental protocols. Biochem. Biophys. Acta **1367**: 88–106. doi:10.1016/S0005-2728(98)00135-2

Kottmeier, D. M., S. D. Rokitta, and B. Rost. 2016*a*. Acidification, not carbonation, is the major regulator of carbon fluxes in the coccolithophore *Emiliania huxleyi*. New Phytol. **61**: 2045–2057. doi:10.1002/lno.10352

Kottmeier, D. M., S. D. Rokitta, and B. Rost. 2016*b*. H^+-driven increase in CO_2 uptake and decrease in HCO_3^-uptake explain coccolithophores' acclimation responses to ocean acidification. Limnol. Oceanogr. **61**: 2045–2057. doi:10.1002/lno.10352

Krause, G., and E. Weis. 1991. Chlorophyll fluorescence and photosynthesis: The basics. Annu. Rev. Plant Biol. **42**: 313–349. doi:10.1146/annurev.pp.42.060191.001525

Kvernvik, A. C., and and others. 2018. Fast reactivation of photosynthesis in arctic phytoplankton during the polar night. J. Phycol. **54**: 461–470. doi:10.1111/jpy.12750

Kvernvik, A. C., and and others. 2020. Higher sensitivity towards light stress and ocean acidification in an Arctic Sea-ice-associated diatom compared to a pelagic diatom. New Phytol. **226**: 1708–1724. doi:10.1111/nph.16501

Kvernvik, A. C., and and others. 2021. Arctic Sea ice algae differ markedly from phytoplankton in their ecophysiological characteristics. Mar. Ecol. Prog. Ser. **666**: 31–55. doi:10.3354/meps13675

Lacour, T., J. Larivière, J. Ferland, F. Bruyant, J. Lavaud, and M. Babin. 2018. The role of sustained photoprotective non-photochemical quenching in low temperature and high light acclimation in the bloom-forming Arctic diatom *Thalassiosira gravida*. Frontiers Marine Sci. **5**: 354. doi:10.3389/fmars.2018.00354

Lannuzel, D., and and others. 2020. The future of Arctic sea-ice biogeochemistry and ice-associated ecosystems. Nature Climate Change **10**: 983–992. doi:10.1038/s41558-020-00940-4

Lewis, K. M., and and others. 2018. Photoacclimation of arctic ocean phytoplankton to shifting light and nutrient limitation. Limnol. Oceanogr. **64**: 284–301. doi:10.1002/lno.11039

Li, G., and D. A. Campbell. 2013. Rising CO_2 interacts with growth light and growth rate to alter photosystem II photoinactivation of the coastal diatom *Thalassiosira pseudonana*. PLoS ONE **8**: e55562. doi:10.1371/journal.pone.0055562

MacIntyre, H. L., T. M. Kana, T. Anning, and R. J. Geider. 2002. Photoacclimation of photosynthesis irradiance response curves and photosynthetic pigments in microalgae and cyanobacteria. J. Phycol. **38**: 17–38. doi:10.1046/j.1529-8817.2002.00094.x

Martin-Jézéquel, V., M. Hildebrand, and M. A. Brzezinski. 2000. Silicon metabolism in diatoms: Implications for growth. J. Phycol. **36**: 821–840. doi:10.1046/j.1529-8817.2000.00019.x

Maturilli, M., I. Hanssen-Bauer, R. Neuber, M. Rex, and K. Edvardsen. 2019. The atmosphere above Ny-Ålesund: Climate and global warming, ozone and surface UV radiation, p. 23–46. *In* H. Hop and C. Wiencke [eds.], The ecosystem of Kongsfjorden, Svalbard. Springer International Publishing.

McMinn, A., M. N. Müller, A. Martin, and K. G. Ryan. 2014. The response of Antarctic Sea ice algae to changes in pH and CO_2. PLoS ONE **9**: e86984. doi:10.1371/journal.pone.0086984

McQuoid, M. R., and L. A. Hobson. 1996. Diatom resting stages. J. Phycol. **32**: 889–902. doi:10.1111/j.0022-3646.1996.00889.x

Mehrbach, C., C. H. Culberson, J. E. Hawley, and R. M. Pytkowicz. 1973. Measurement of the apparent dissociation constants of carbonic acid in seawater at atmospheric pressure. Limnol. Oceanogr. **18**: 897–907. doi:10.4319/lo.1973.18.6.0897

Melnikov, I. A., E. G. Kolosova, H. E. Welch, and L. S. Zhitina. 2002. Sea ice biological communities and nutrient dynamics in the Canada Basin of the Arctic Ocean. Deep-Sea Res. I Oceanogr. Res. Pap. **49**: 1623–1649. doi:10.1016/S0967-0637(02)00042-0

Melzner, F., F. C. Mark, B. A. Seibel, and L. Tomanek. 2020. Ocean acidification and coastal marine invertebrates: Tracking CO_2 effects from seawater to the cell. Ann. Rev. Mar. Sci. **12**: 499–523. doi:10.1146/annurev-marine-010419-010658

Moejes, F. W., and and others. 2017. A systems-wide understanding of photosynthetic acclimation in algae and higher plants. J. Exp. Bot. **68**: 2667–2681. doi:10.1093/jxb/erx137

Nicolaus, M., C. Katlein, J. Maslanik, and S. Hendricks. 2012. Changes in Arctic Sea ice result in increasing light transmittance and absorption. Geophys. Res. Lett. **39**: L24501. doi:10.1029/2012GL053738

Oxborough, K., C. M. Moore, D. J. Suggett, T. Lawson, H. G. Chan, and R. J. Geider. 2012. Direct estimation of functional PSII reaction center concentration and PSII electron flux on a volume basis: A new approach to the analysis of fast repetition rate fluorometry (FRRf) data. Limnol. Oceanogr.: Methods **10**: 142–154. doi:10.4319/lom.2012.10.142

Pelusi, A., F. Margiotta, A. Passarelli, M. I. Ferrante, M. Ribera d'Alcalà, and M. Montresor. 2020. Density-dependent mechanisms regulate spore formation in the diatom *Chaetoceros socialis*. Limnol. Oceanogr.: Letters **5**: 371–378. doi:10.1002/lol2.10159

Pierrot, D. E., E. Lewis, and D. W. R. Wallace. 2006. MS Exel Program Developed for CO_2System Calculations. *In* O. R. N. L.ORNL/CDIAC-105aCarbon Dioxide Information Analysis Centre [ed.].

Platt, T., C. Gallegos, and W. Harrison. 1980. Photoinhibition of photosynthesis in natural assemblages of marine phytoplankton. J. Mar. Res. **38**: 687–701.

Poulin, M., G. J. C. Underwood, and C. Michel. 2014. Sub-ice colonial *Melosira arctica* in Arctic first-year ice. Diatom Res. **29**: 213–221.

Prosser, J. I., and and others. 2007. The role of ecological theory in microbial ecology. Nat. Rev. Microbiol. **5**: 384–392. doi:10.1038/nrmicro1643

R Core Team 2017. R: A language and environment for statistical computing. R Foundation for Statistical Computing, Vienna, Austria. URL https://www.R-project.org/

Rokitta, S. D., U. John, and B. Rost. 2012. Ocean acidification affects redox-balance and ion-homeostasis in the life-cycle stages of *Emiliania huxleyi*. PLoS ONE **7**: e52212. doi:10.1371/journal.pone.0052212

Rokitta, S. D. S. A. Kranz, and B. Rost. 2022. Inorganic carbon acquisition by aquatic primary producers / S. Marbely and B. Gontero (editors), In: Blue Planet, Red and Green Photosynthesis, London, ISTE-Wiley, 81-114, ISBN: 9-781-78945-082-8

Rost, B., S. A. Kranz, K.-U. Richter, and P. D. Tortell. 2007. Isotope disequilibrium and mass spectrometric studies of inorganic carbon acquisition by phytoplankton. Limnol. Oceanogr.: Methods **5**: 328–337. doi:10.4319/lom.2007.5.328

Rost, B., K.-U. Richter, U. L. F. Riebesell, and P. J. Hansen. 2006*a*. Inorganic carbon acquisition in red tide dinoflagellates. Plant, Cell Environ. **29**: 810–822. doi:10.4319/lom.2007.5.328

Rost, B., U. Riebesell, and D. Sültemeyer. 2006*b*. Carbon acquisition of marine phytoplankton: Effect of photoperiod length. Limnol. Oceanogr. **51**: 12–20. doi:10.4319/lo.2006.51.1.0012

Seifert, M., B. Rost, S. Trimborn, and J. Hauck. 2020. Meta-analysis of multiple driver effects on marine phytoplankton highlights modulating role of pCO_2. Glob. Chang. Biol. **26**: 6787–6804. doi:10.1111/gcb.15341

Søreide, J. E., E. Leu, J. Berge, M. Graeve, and S. Falk-Petersen. 2010. Timing of blooms, algal food quality and *Calanus glacialis* reproduction and growth in a changing Arctic. Glob. Chang. Biol. **16**: 3154–3163. doi:10.1111/j.1365-2486.2010.02175.x

Southwood, T. R. E., R. M. May, M. P. Hassell, and G. R. Conway. 1974. Ecological strategies and population parameters. Am. Nat. **108**: 791–804. doi:10.1086/282955

Spilling, K., P. Ylöstalo, S. Simis, and J. Seppälä. 2015. Interaction effects of Light, temperature and nutrient limitations (N, P and Si) on growth, stoichiometry and photosynthetic parameters of the cold-water diatom *Chaetoceros wighamii*. PLOS ONE **10**: e0126308. doi:10.1371/journal.pone.0126308

Stoll, M. H. C., K. Bakker, G. H. Nobbe, and R. R. Haese. 2001. Continous-flow analysis of dissolved inorganic carbon content in seawater. Anal. Chem. **73**: 4111–4116. doi:10.1021/ac010303r

Strobel, A., M. Graeve, H. O. Poertner, and F. C. Mark. 2013. Mitochondrial acclimation capacities to ocean warming and acidification are limited in the Antarctic Nototheniid fish, *Notothenia rossii* and *Lepidonotothen squamifrons*. PLOS ONE **8**: e68865. doi:10.1371/journal.pone.0068865

Syvertsen, E. E. 1991. Ice algae in the Barents Sea: Types of assemblages, origin, fate and role in the ice-edge phytoplankton bloom. Polar Res. **10**: 277–288. doi:10.1111/j.1751-8369.1991.tb00653.x

Thompson, P. A., P. J. Harrison, and J. S. Parslow. 1991. Influence of irradiance on cell volume and carbon quota for ten species of marine phytoplankton. J. Phycol. **27**: 351–360. doi:10.1111/j.0022-3646.1991.00351.x

Timmermans, M., C. Ladd, and K. Wood. 2015. Sea surface temperature. Arctic Report Card: 41–43.

Torstensson, A., and and others. 2021. Sea-ice microbial communities in the Central Arctic Ocean: Limited responses to short-term pCO2 perturbations. Limnol. Oceanogr. **66**: S383–S400. doi:10.1002/lno.11690

Van de Waal, D. B., and and others. 2019. Highest plasticity of carbon-concentrating mechanisms in earliest evolved phytoplankton. Limnol. Oceanogr. Lett. **4**: 37–43. doi:10.1002/lol2.10102

van Leeuwe, M., and and others. 2018. Microalgal community structure and primary production in Arctic and Antarctic Sea ice: a synthesis. Elem. Sci. Anth. **6**: 4. doi:10.1525/elementa.267

von Quillfeldt, C. H. 2000. Common diatom species in Arctic spring blooms: Their distribution and abundance. Bot. Mar. **43**: 499–516. doi:10.1515/bot.2000.050

Wadhams, P. 2012. Arctic ice cover, ice thickness and tipping points. Ambio **41**: 23–33. doi:10.1007/s13280-011-0222-9

White, E., C. J. M. Hoppe, and B. Rost. 2020. The Arctic picoeukaryote *Micromonas pusilla* benefits from ocean acidification under constant and dynamic light. Biogeosciences **17**: 635–647. doi:10.5194/bg-17-635-2020

Wolf, K. K. E., and and others. 2019. Company matters: The presence of other genotypes alters traits and intraspecific selection in an Arctic diatom under climate change. Glob. Chang. Biol. **25**: 2869–2884. doi:10.1111/gcb.14675

Wolf, K. K. E., C. J. M. Hoppe, and B. Rost. 2018. Resilience by diversity: Large intraspecific differences in climate change responses of an Arctic diatom. Limnol. Oceanogr. **63**: 397–411. doi:10.1002/lno.10639

Young, J. N., J. A. Goldman, S. A. Kranz, P. D. Tortell, and F. M. Morel. 2015. Slow carboxylation of Rubisco constrains the rate of carbon fixation during Antarctic phytoplankton blooms. New Phytol. **205**: 172–181. doi:10.1111/nph.13021

Young, J. N., and K. Schmidt. 2020. It's what's inside that matters: Physiological adaptations of high-latitude marine microalgae to environmental change. New Phytol. **227**: 1307–1318. doi:10.1111/nph.16648

Zhang, Y., M. Yamamoto-Kawai, and W. J. Williams. 2020. Two decades of ocean acidification in the surface waters of the Beaufort gyre, Arctic Ocean: Effects of sea ice melt and retreat from 1997–2016. Geophys. Res. Lett. **47**: e60119. doi:10.1029/2019GL086421

Acknowledgments

The authors would like to thank Eva Husmann for her committed assistance during the lab phase of this experiment and her participation in cell counts of *M. arctica* cultures. They also acknowledge the invaluable experience and help of Klaus-Uwe Richter during measurements and troubleshooting at the MIMS. They furthermore thank Philipp Assmy and Marit Reigstad for their evaluation of resting stages of *M. arctica*, and Eva-Maria Noetig for sharing a valuable assortment of literature on *M. arctica* ecology. Finally, they would like to thank A. Stecher for providing the *M. arctica* strain. This study was funded by the Alfred-Wegener-Institut Helmholtz-Zentrum fur Polar- und Meeresforschung. Open Access funding enabled and organized by Projekt DEAL.

Conflict of Interest

The autors declare no conflit of interest.

Submitted 26 December 2021
Revised 02 June 2022
Accepted 04 June 2022

Associate editor: Maren Striebel